Improvement of thermal energy accumulation by incorporation of carbon nanomaterial into magnesium chloride hexahydrate and magnesium nitrate hexahydrate

Pavla Honcová[1], Galina Sádovská[1,2], Jana Pastvová[2], Petr Koštál[1], Jürgen Seidel[3], Petr Sazama[2], Radim Pilař[2]

[1]Faculty of Chemical Technology, University of Pardubice, Doubravice 41, 53210 Pardubice, Czech Republic
[2]J. Heyrovský Institute of Physical Chemistry, Academy of Science of the Czech Republic, Dolejskova 3, 182 23 Praha 8, Czech Republic
[3]Institute of Physical Chemistry, TU Bergakademie Freiberg, Leipziger Str. 29, 09596 Freiberg, Germany

Abstract

Magnesium chloride hexahydrate and magnesium nitrate hexahydrate were tested for thermal energy storage in mixture with different carbon materials. The graphite, graphene, and zeolite-templated carbon replicas were used as a nucleating agent supressing supercooling. The addition of any carbon into magnesium chloride hexahydrate did not lead to decrease of the supercooling, and the significant decrease of the enthalpy of fusion and crystallization was observed. The mixtures after cycling were apparently wet, indicating that some of the magnesium chloride was dissolved in its structural water. In the case of magnesium nitrate hexahydrate, the addition of carbon replica of zeolite beta with various Si/Al ratios, mordenite or faujasite lead to decrease of supercooling. Nevertheless, graphite and graphene provided the highest supercooling suppression from about 30 to 2.2 K within the fifty cycles (heating-cooling). The measurement of pressed tablets at 5 MPa of magnesium nitrate hexahydrate with carbon materials showed significant increase of the thermal conductivity of 9 % and 15 % for the addition of 3 mass% of graphene and 3 mass% of graphite, respectively. Mixing of magnesium nitrate hexahydrate with graphene or graphite improved heat transfer and significantly reduced unwanted supercooling, which is necessary for use for the thermal energy accumulation.

Keywords:

Phase change materials, Supercooling, Zeolite-templated carbon replica, Graphite, Graphene

1. Introduction

An effort to reduce the natural raw material consumption together with the discrepancy between the supply and demand of energy from renewable sources leads to request for long-term energy storage. Phase change materials (PCMs) seem to be suitable candidates for this task and several salt hydrates have been explored extensively [1-3]. However, the large-scale implementation of PCMs into the energy system is still lacking and requires significant improvement of proposed PCMs. The main demands of PCM are: low price, non-toxicity and its stability over thousands of phase change

cycles. In the case of phase change cycles (including melting-crystallization in the case of salt hydrates) there are two main aspects negatively influencing its repeatability and stability. One of them is the separation of the phases which could be overcome by encapsulation [4-6] or by addition of filler which sterically prevent from separation [7]. The second aspect is the supercooling – the temperature of the phase change during the charging is higher than the temperature of the phase change during the discharging. The suppression of supercooling is one of the most important steps on the way to practical application and obviously is trying to be solved by addition of nucleating agent [7-12]. Nevertheless, there is another problem with heat transfer caused by low thermal conductivity which is not optimal for many of promising PCMs [3, 5, 10, 13-16]. This could be again overcome by encapsulation [5, 17] or addition of better thermal conducting material into the PCMs as have been tested for graphite [18-20], carbon nanomaterial [21], graphene oxide [22], silver [23], copper [24, 25], etc. Cabeza et al. [26] observed that the thermal conductivity of water was improved by graphite more than by copper. However, the best from the supercooling and thermal conductivity points of view is improving of both the aspects at once by addition of carbon materials as a phase separation prevention and nucleating agent with third positive effect comprising increase of the thermal conductivity of PCM material.

The aim to improve thermal conductivity of phase change materials can be divided into two directions. Either is the phase change material arrange into the high thermal conductive system (stationary structure consist of foam, fibre, wire, sheets or tube net; encapsulation) or the high conductive material is uniformly distributed in PCM [3, 5, 19, 25, 27-31]. Metals have high thermal conductivity [14, 25, 27] but they can undergo corrosion especially in the case of inorganic salt hydrates [3, 32-34]. On the other hand, carbon materials are resistive to corrosion and their thermal conductivity is higher in comparison to PCMs [14, 25, 35]. Furthermore, introduction of highly conductive material into PCM and creation of composite is a straightforward solution. In the case of organic PCMs the addition of graphite [18, 29, 36], expanded graphite [19, 37, 38], graphene [29], graphene oxide [22], active carbon [39], multi-walled carbon nanotubes [21, 40-42] or nanofibers [21, 25, 43] were tested not only for waxes [19, 21, 25, 40, 43], but also for other presumptive PCMs [18, 22, 25, 36, 37, 39, 41, 42] and the improving of thermal conductivity was observed. In the case of inorganic salts hydrates the expanded graphite was added to magnesium chloride hexahydrate [44] or calcium chloride hexahydrate [45-47]. The composite consists of either expanded graphite or expanded graphite oxide and eutectic mixture of $Na_2CO_3·10H_2O$ and $Na_2HPO_4·12H_2O$ was studied by Liu and Yang [48]. The addition of carbon powder into $Na_2HPO_4·12H_2O$ was studied by Ryu et al. [7]. The results of addition of carbon fibres in $Na_2SO_4·10H_2O$ was published by Fukai et al. [49] and for $Mg(NO_3)_2·6H_2O – MgCl_2·6H_2O – NH_4NO_3$ eutectic mixture by Frusteri et al. [50]. Wu et al. [51] added expanded graphite modified by titanium into $KAl(SO_4)_2·12H_2O$ together with magnesium chloride hexahydrate as nucleator and showed the increase in thermal conductivity and stability of this composite. In some case the surfactant was added to improved wettability of carbon with melted inorganic salt [7, 44]. In almost all cases the addition of carbon into PCM lead to suppression of supercooling (in the case of data published by Ye at al. [46] the nucleating agent had to be added) and improving of thermal conductivity, nevertheless the addition of surfactant can decrease the thermal conductivity [45].

The salts as magnesium chloride hexahydrate (referred as MCH in following text) and magnesium nitrate hexahydrate (referred as MNH) seem to be perspective materials for thermal energy storage in the medium temperature interval. The accumulation ability of magnesium salt hydrates, especially of MCH and MNH has been already

published [8, 9, 11, 52] where the melting temperature is 117.2 [52] and 89.7 °C [53] and enthalpy of fusion of 34.6 [52] and 40.8 kJ/mol [53] for MCH ("quasi-congruent melting" as peritectic point and the incongruent melting point are only separated by 0.7 mass% $MgCl_2$ [54] and MNH (congruent melting [54]), respectively. Unfortunately, both pure salts exhibit huge supercooling which must be suppressed before any practical application. The literature reported supercooling is for both salts about 30 K [8, 52] and thermal conductivity only 0.694 W/m K (solid, 90 °C) and 0.611 W/m K (solid, 37 °C) for MCH and MNH, respectively [3].

This work is focused on the significant decrease of supercooling as well as improving of the thermal conductivity of MCH and MNH by addition of carbon material differing in structure.

2. Materials and Methods

Magnesium nitrate hexahydrate (99.0 %, Lach-Ner Ltd.) and magnesium chloride hexahydrate (99.0 %, PENTA) were mixed with different carbon powders. The carbon material was either specially synthesized (5 zeolite-replica carbon samples) or commercially available graphite (98 %, 200 mesh ultrafine, Jinkuancheng Carbon) and graphene (98 %, 1-5 layers, Graphene Epoxies). Carbon nanomaterials were mixed with MCH or MNH in solid state using the agate mortar and the total mass of mixture was about 0.5 g. In all cases the mixtures were dry (i.e. any wetting of mixture was not observed), and well dispersed without any conglomerates.

2.1 Synthesis of carbon samples

Five zeolite-replica carbon samples were synthesized in zeolites as hard templates for preparation of 3D graphene-like structure. The commercial beta zeolite (*BEA/11.3; Si/Al = 11.3, Zeolyst Int.), faujasite (FAU; Si/Al = 6, Zeolyst Int.), mordenite (MOR; Si/Al = 12, Zeolyst Int.), synthetized Al-rich beta zeolite (*BEA/5.6; Si/Al = 5.6) were used as microporous or after desilication as micro-mesoporous template. Carbonization of zeolites was performed using chemical vapour deposition with propylene or furfuryl alcohol (FA) as a carbon precursor, followed by dissolution of the zeolite framework with HF and HCl acids. Besides, before carbonization, the *BEA/11.3 and MOR zeolites were desilicated to obtain the mesopores. The *BEA/11.3 zeolite was prepared by treatment in alkaline solutions (30 ml 0.3 M NaOH per 1 g of zeolite, stirring in a beaker at 65 °C for 30 min). The MOR zeolite was desilicated by alkaline solution (30 ml 0.2 M NaOH per 1 g of zeolite, stirring in a beaker at 85 °C for 2 h) and then dealuminated by acid solutions (100 ml 0.5 M $(COOH)_2$ per 1 g of zeolite, stirring in a beaker at 80 °C for 20 h). Prepared micro-mesoporous *BEA/11.3 and MOR zeolites indexed "m" were used as a template for β_{11m}-C and M_m-C samples, respectively. Al-rich beta zeolite *BEA/5.6 was hydrothermally synthesized from aluminosilicate synthesis gel and used for preparation of carbon material denoted as β_6-C. Carbonization of sample β_{11}-C, β_{11m}-C, Y-C and M_m-C was done using the chemical vapour deposition with propylene as a carbon precursor. The appropriate zeolite was placed in a quartz reactor, activated at 750 °C for 1 h at a heating rate of 3 °C min^{-1} under a flow of helium, carbonised in a propylene stream (5 vol.% in He) for 2 h at 750 °C. Then the propylene stream was switched to a stream of helium and temperature was increased to 900 °C for 3 h at a heating rate of 3 °C min^{-1}. Carbon β_6-C was prepared by impregnation of Al-rich *BEA/5.6 with FA (3 ml FA per 3 g of zeolite at 90 °C for 3 days), subsequently was carbonised at 200 °C for 3 h and then 900 °C for 3 h under a flow of helium (heating rate of 3 °C min^{-1}). The zeolite was in all cases removed from the carbon/zeolite composite by leaching using a large excess of aqueous

solutions of hydrofluoric and hydrochloric acids (the zeolite/carbon composite was stirred in a beaker with 350 ml 5 mass% HF solution at room temperature for 5 h, then with 50 ml 42 mass% HF solution for 1 h, and finally with 30 ml 37 mass% HCl solution for 1 h). The resulting carbon sample was isolated by repeated centrifugations and washing with a large volume of water and by filtration. Obtained material was dried in air at 120 °C for 12 h. The synthesis is described in detail elsewhere [55].

2.2 Characterization of samples

The characterization of carbon materials was done using X-ray powder diffraction (XRD), scanning electron microscopy (SEM) the surface area measurement and thermal analysis measurement. The magnesium hydrate salts either pure or as a mixture with carbon material were characterised by XRD, optical microscopy, thermal analysis measurement, thermal conductivity measurement and density measurement. The X-ray powder diffraction patterns were obtained using a Bruker AXSD8 Advance diffractometer with CuK$_\alpha$ radiation. The scans were taken over scattering angles 2θ from 5° to 90°.

Scanning electron microscope JEOL JSM-03 was used to imagine the morphology, shape and size of carbon materials. The surface area of carbon materials was determined by analysis of the adsorption isotherms of nitrogen using the BET theory and ASAP2010 apparatus (Micromeritics).

The combustion point of carbon materials was determined by thermal analysis using TG/DSC 111 (Setaram) and the heating rate of 5 K/min was applied in the temperature range from 25 to 700 or 800 °C in atmosphere of argon with 20 % of oxygen on 4 mg sample. The heat capacity of selected samples at temperature of 25 °C was determined using calorimeter C80 (Setaram) and the stepwise method [56, 57]. The uncertainty of C_p determination is 0.5 %.

The optical microscope Olympus BX51 with DP72 camera was used to observe samples before and after DSC experiments (micrographs were taken in transmission mode).

Thermal conductivity of selected samples was measured using thermal conductivity analyser TCi (C-Therm; based on the Modified transient plane source technique) placed in thermal chamber Tenney (TPS). The instrument based on modified transient plane source needs samples with the plane surface and diameter at least 17 mm. The primary measured value is effusivity, e, which can be recalculated into thermal conductivity k using the density ρ and the heat capacity C_p value as $k = e^2/(\rho \cdot C_p)$. However, both effusivity and thermal conductivity have their own internal calibration differing for each material groups and power levels reflecting voltage changes in time during the measurement [58]. The error of k determination is 5 %. The thermal conductivity was determined for MNH in the temperature range of 10 – 50 °C as well as for the mixture of MNH with 3 mass% of promising admixture at 25 °C. The samples of MNH for thermal conductivity measurement were in the form of a disc prepared either as pellet pressed using 1, 2 and 5 MPa (using apparatus BSML11 Brio) or a moulded tablet prepared by solidification of MNH melt in the mould without any pressing. For these samples silicon thermal grease has to be used to have good thermal contact between the sample and the sensor. Moreover, also the samples in the form of powder (crystalline MNH, selected carbon materials or MNH with carbon materials mixed in agate mortar) were measured without any contact agent. The temperature dependence of density [59] (Eq. 1) and heat capacity [53] (Eq. 2) from

literature or experimental data were used to recalculate effusivity into thermal conductivity for pure MNH in the compact form:

$$\rho = 1.756 - 0.0004\,T \quad (\text{g/cm}^3) \tag{1}$$

$$C_p = 1115 - 6.5\,T + 0.0143\,T^2 \quad (\text{J/mol K}) \tag{2}$$

where T is a temperature in K. In the case of selected carbon materials and MNH with carbon materials in the form of powder the density was determined for temperature of 25 °C as a bulk density (ρ_b) or tapped density (ρ_t). The bulk density was determined using helium Autopycnometer 1320 (Micromeritics) and the uncertainty of density determination is 1 %. The tapped density was obtained by mechanically tapping a graduated measuring cylinder (5 ml volume) containing the powder sample. The mechanical tapping was achieved by raising the cylinder leading to dropping of the sample under its own mass until little further volume mass change was observed. The tapped density corresponds to the form of powder sample measured by TCi. The density of samples in compact form (ρ_c) prepared as pellets and compact moulded tablets with regular shape was determined as sample mass divided by its calculated volume.

2.3 Thermal energy accumulation tests

The ability of thermal energy accumulation was tested using differential scanning calorimetry (DSC). Pure salt hydrates were analysed within the four cycles of heating/cooling scan as well as their mixtures with 3 mass% of selected carbon material utilizing DSC 111 (Setaram) where the heating rate was 4 K/min and the cooling rate of 2 K/min in the temperature range of 30 - 170 °C for MCH and 25 - 130 °C for MNH based samples; sample mass about 30 mg was used (referred as slow cycles in following text). Based on these few slow cycles the promising mixtures were tested during 50 cycles of heating/cooling scan done by rate of 10 K/min using DSC Pyris 1 (Perkin Elmer), where the sample mass was about 10 mg. The promising mixture of MNH with carbon was further tested on compositions with 0.5, 1, 2 and 3 mass%. Both differential scanning calorimeters were calibrated using melting temperature of several metals (Hg, Ga, In, Sn, Pb and Zn) and the enthalpy change was calibrated using the heat of fusion of indium (28.45 J/g).

3. Results and Discussion

The main results of carbon samples' synthesis and basic characterization are given in Tab. 1. X-ray diffraction analysis of carbon materials confirmed zeolite replica structures (see Ref. [55]). The parent zeolites differ in inner channel dimensions forming accessible volume for carbon deposition, being 12.27, 20.52 and 27.42 % for MOR, *BEA and FAU [60], respectively. Some carbon replica's surface area is higher than hypothetical values of parent zeolite accessible area calculated from ideal framework 1000-1200 m²/g due to defects in structure. Using of mesoporous zeolite template led to formation of 3D-carbon with lower surface area but with channels that are more accessible. The largest specific surface area higher than 2400 m²/g was determined for graphene, β_{11}-C and Y-C samples. On the contrary, the lowest value 8 m²/g was measured for graphite. The specific surface of the other carbons is in the interval 400 – 1500 m²/g.

The range of crystal size was calculated from SEM (Supporting information in [55]) photographs. The zeolite replica carbons showed nanoparticles with diameter from 200 – 1000 nm. The graphite and graphene showed layered plate-like particles with larger size of 3-100 μm, but the thickness of < 40 nm.

The calorimetric study started with the determination of supercooling of the tested salts at the given experimental conditions. DSC traces of pure salt hydrates in slow four cycles are given in Fig. 1. Both results illustrate that the melting is observed as a broad endothermic effect whereas crystallization gives a sharp exothermic effect. In the case of MNH there is an additional small effect at a temperature of about 65 – 75 °C corresponding to the solid-solid phase transition [8, 53]. Moreover, the shape and position of DSC peaks for the first heating/cooling scans are different compared to others. This reflects different sample form – during the first heating scan the sample is in the form of separated crystals surrounded by air freely lying on the crucible bottom up to the melting; the compact form is creating after the melting and during the consequent cooling. Therefore, the first cycle was not taken into account for the average values given in the Results and discussion part for all DSC measurements. The enthalpy of fusion (ΔH_f) and crystallization (ΔH_{cr}) is determined from the area below the DSC peak (pure salts on Fig. 1). The value of supercooling (ΔT) is the difference between the melting temperature (T_m) and temperature of crystallization (T_{cr}) – both evaluated as an onset temperature as is shown in inserted figure in Fig. 1B. During the four slow cycles some changes of peak position and shape can be observed (Fig. 1). The melting point of pure salts (Ref. [52] for MCH and [53] for MNH) obtained by heating rate of 10 K/min is emphasized by arrow. In the case of MNH, the shift of (l)-(s) crystallization peak towards lower temperature sometimes caused overlapping of (s)-(s) phase transition peak (1st and 4th cooling scan at Fig. 1B). Thus, the occasional impossibility to separate both effects, the enthalpy change for heating and cooling scans is reported as a sum of both effects during the heating (ΔH_h) and cooling (ΔH_c) in the case of MNH.

Focusing on MCH and its carbon mixtures, the melting appears similarly to pure MCH for mixture with graphite or graphene (Fig. 2). Mixtures of MCH with β_6-C, β_{11}-C, β_{11m}-C or Y-C carbons shows melting peak shift towards the lower temperature with increasing number of cycles. All additives showed significant unfavourable decrease in enthalpy in both heating and cooling directions with lacking decrease of supercooling. Only mixture of MCH with M_m-C displays the most positive increase of T_{cr} with acceptable values of ΔH_{cr}, improved with the number of cycle but the supercooling is still high.

Unfortunately, the results summarised in Fig. 3 clearly shows that the addition of tested carbon nanomaterial into MCH did not distinctly decreased the supercooling but significantly decreased values of enthalpy of fusion and crystallization in all mixtures. Rather, it was observed the increase of supercooling as shown in Supplementary information (Fig. S1) for 3 mass% of Y-C where the position of crystallization peak is shifted with the number of cycles toward lower temperatures while the melting peak remains at similar temperature. Whilst the position of crystallization peak remains at similar temperature and the melting peak changes with the number of cycles for β_6-carbon (Fig. S2). Thus, the addition of carbon nanomaterial into MCH is not suitable as a nucleating agent and any further measurements were not performed. In this case the formation of lower MCH hydrates is assumed as a reason for changes in enthalpy. The appearance of the samples as wet crystals after cycling suggests this assumption. Therefore, the X-ray diffraction analysis was performed to identify newly formed solid phases. The strongest lines were sought for magnesium chloride tetrahydrate (MCT), dihydrate (MCD), anhydrous (MC) and magnesium hydroxyl-chloride (MHC), however no other crystalline phase than MCH were identified by crystal phase analysis in

diffractograms. Even when sample was frozen in the XRD holder to allow all the components to crystallize, only an amorphous phase was observed as a broad hump on XRD curve. Supplementary information contain table (Table S1) with characteristic lines and some examples of diffractogram (Fig. S3).

During the first heating of MNH, the endothermic (s)-(s) phase transition occurs and then the melting is reflected as a second endothermic effect (see Fig. 1B). In the following cooling scan firstly, the crystallization occurs followed by (s)-(s) phase transition, but both effects can overlap and create complex effect. However, in the case of all mixtures of MNH with carbon no overlapping of crystallization and (s)-(s) phase transition peaks was observed. Moreover, the peak of (s)-(s) phase transition was the same for all cycles except of the mixture with β_{11}-C where the transition peak was during the first cooling scan shifted to the higher temperature compared to the following cycles. Concerning melting, pure MNH as well as its mixture with graphite, graphene, β_6-C or M_m-C (Fig. 4A) shows the melting peak for the first cycle higher than during the other cycles, where the others have similar shape and gives similar value of T_m (as is illustrated in Fig. 1B). Mixtures of MNH with β_{11}-C, β_{11m}-C and Y-C shows shift of melting peak towards lower temperature with increasing number of the cycle and the height of the peak is for the first cycle lower compared to other cycles. The crystallization peak without any change with number of cycles is observed for the mixture with graphene. Illustration of crystallization peaks for MNH and its mixtures is given in Fig. 4B. The values of enthalpy of fusion, crystallization and supercooling for materials tested in four slow cycles are summarised in Fig. 5. Comparing slow four cycles of pure MNH to the fast ones (published in [8]) the similar value of ΔH_f was obtained, a bit higher value of ΔH_{cr} and lower value of ΔT, which is 19.3 °C for slow cycles compared to 28.5 °C from the fast four cycles. The real condition of charge/discharge with slow cooling rate will provide enough time to material crystallization thus crystallization will occur at higher temperature with decreased supercooling.

Taking into account the enthalpy of phase changes and supercooling of fast 4 cycles shown in Fig. 5, the best results were achieved by a mixture of MNH with graphite, M_m-C, graphene and β_6-C. Additional tests were performed for these three compositions with variable carbon content of 0.5 - 3 mass% throughout fifty fast cycles. The final values are summarised in Fig. 6 together with data for pure MNH published in [8]. The examples of DSC curves obtained during the cycling of two most promising materials are given in Fig. 7 and show broad melting peaks. But the significant difference was in the crystallization peak, where narrow sharp and high crystallization peak was observed for mixture of MNH with 0.5 and 3 % of M_m-C, 0.5 % of GREN, 0.5 % of GRIT and 1 – 3 % of β_6-C. On the contrary, the broad crystallization peaks similar to melting peak was observed for mixture with 1 – 3 % of GRIT.
The value of enthalpy of fusion and crystallization for all tested mixtures is similar to pure MNH or slightly higher. However, supercooling is much greater for the mixture with all tested concentrations of β_6-C than for pure MNH. This huge difference between supercooling observed for four slow cycles and fifty fast cycles is not only due to the different rates, but also due to the number of performed cycles. At the beginning of the fast cycles the supercooling is about 5 °C, but around 5th or 10th cycle (25 in the case of 0.5 mass% addition) significantly increased. Similar behaviour was observed for

mixture with 3 mass% of M_m-C. On the contrary, the mixture with 2 mass% of M_m-C provided low supercooling throughout the cycling except the first cycle as is depicted in Fig. 7A. Generally, the zeolite-templated carbon replicas are hydrophobic, therefore the contact of nanoparticles with melted salt is limited. Further research to improve nano-structured 3D carbon to become more wettable is necessary. In contrary GREN and oxidized GRIT are more hydrophilic which helps to spread the melt into the 2D structure and consequently facilitates contact with solid surface and promotes crystallization of MNH. The addition of 0.5 mass% of GRIT and even more of GREN do not lead to significant decrease of ΔT but higher content of these components brought the desired result. Taking into account both the enthalpy of phase transitions and supercooling (see Fig. 6), the best results were achieved by a mixture of MNH with 2 mass% of GRIT (illustration of DSC curves is given in Fig. 7B) or with 3 mass% of GREN.

Although the addition of graphite or graphene into MNH significantly decreased supercooling and their mixtures withstand 50 cycles giving excellent results the attention must be paid to carbon wettability in MNH. Practical application of PCM material requires working life over thousands of cycles where the gradual phase separation can cause decrease of thermal energy storage. The optical microscopy was used to observe homogeneity of the samples after DSC heating/cooling tests in 4 slow cycles as well as 50 fast cycles. Selected pictures are given in Fig. 8. In all cases, the carbon particles were mainly on the surface of the sample but there were also particles in the volume of the sample as is depicted in Fig. 8A. However, in the case of mixture with M_m-C the concentration of carbon on the surface leads to formation of separated layer (thicker on the sample top and thinner on the sample bottom) as can be seen in Fig. 8B. These results emphasize the next necessary step for successful carbon material implementation into long working salt hydrate thermal storage system. Though carbon material suppressed supercooling while maintaining sufficiently large enthalpy change, its hydrophobic properties lead to the phase separation. Thus, modification of carbon to improve its wettability is critical for commercial application.

The thermal conductivity belongs to the most important physical properties of PCMs together with the temperature of the phase change and the value of its enthalpy change. In the case of inorganic salt hydrates, the thermal conductivity is rarely published, especially for liquid state [27]. The thermal conductivity of MNH and of its promising mixtures with 3 mass% of graphite and graphene was determined for temperature of 25 °C for both powder and compact form. The value of density and heat capacity is necessary to determine the thermal conductivity. The measured values of effusivity, density and heat capacity with calculated thermal conductivity are given in Table 2 and Table 3 for samples in the powder and compact form, respectively.

The heat capacity of MNH was already published [53], thus only C_p values for GRIT, GREN and their mixtures with MNH were determined. Both carbon materials have a low C_p close to each other, thus the heat capacity for their mixtures with MNH are similar and slightly lower in comparison to pure MNH. In the case of powder sample, the bulk density of MNH corresponds to 1637 kg/m^3 published by Kenisarin and Mahkamov [59] calculated using Eq. (1). The bulk density of graphite is a bit higher than that of graphene, but both are higher than for MNH. Therefore, the density of mixtures for both carbons is slightly higher than for pure MNH. The tapped density covers also the free volume among the particles, so the particle size and shape can affect the rheological properties and change the resulting value of tapped density.

Smaller particles have better ability to rearrange during the tapping leading to higher tapped density as is clear from results given in Table 2. Thus, mixtures of MNH with carbons (the mixtures contain MNH with smaller particle size corresponding to data marked with ** in Table 2) have a bit lower tapped density than pure MNH. The bulk density does not correspond to the form of the sample for thermal conductivity test, thus the tapped density was included in the calculation. As can be expected, the thermal conductivity of the powder samples is very low because there is a large influence of free volume filled by air among the particles. Smaller particles have better ability to rearrange and reduce the free volume in comparison to bigger one, thus the effusivity and thermal conductivity is higher. In the powder form, the thermal conductivity of GRIF and GREN is comparable with smaller particles of MNH. However, the mixtures of MNH with carbons have higher e and k because of reduced free volume by immersion of carbon.

For practical application, the compact form of PCM is used resulting from a repeated (l) – (s) transformation. Knowledge of the thermal conductivity of PCM in working temperature range allows to predict the heat conduction behaviour. Unfortunately, our experimental setup enables to measure MNH sample in temperature range overlapping melting temperature, because the sample located in thermal chamber can gradually dehydrate at higher temperature. That is why the thermal conductivity of MNH was determined in the temperature range of 10 – 50 °C for sample in the compact form differing in applied pressure during tablet preparation. Compact tablets were prepared by solidification of MNH melt in the mould without any pressing (called as moulded sample in following part). Moreover, pellets of MNH were prepared using the pressure of 1, 2 or 5 MPa. Density of compact form (ρ_c given in Table 3) was determined by dividing the sample mass to its volume calculated as regular cylindrical shape. The density of MNH in the form of pellets prepared using the pressure of 5 MPa is close to value determined by helium pycnometer at temperature of 25 °C (see Table 2 and Table 3). However, pellets of pure MNH prepared using lower pressure and especially moulded sample have significantly lower density. This can be explained by the presence of free volume among the crystals. Consequently, the value of e and k is lower for lower pressure used for pellets preparation and the lowest is for moulded sample. The temperature dependence of k for MNH compact samples is given in Fig. 9 (T_m of pure MNH is emphasized). The moulded sample has quite high error limit of average value of k at given temperature, because there is high dispersion of free volume amount in each prepared sample. That high dispersion also reflects in high error limit of ρ_c value. Nevertheless, the thermal conductivity of moulded sample corresponds well with data published by Zalba et al. [3]. Pellets prepared using different pressure show increase of k – the higher is the pressure the higher is the value of k, but k for 2 MPa is very close to data obtained for 5 MPa (similarly to ρ_c values). The increase of thermal conductivity with higher pressure applied during the preparation of the sample was also published for composites based on erythritol [35]. The temperature dependence of k is in measured temperature range linear for all samples, but the slope slightly increased with increasing pressure as can be seen in Fig. 9 and Table 4. The addition of GREN increased the thermal conductivity, but the increase is even higher for addition of GRIT. However, the improving of thermal conductivity of MNH by the addition of carbon in order of few percent seems not to be obvious as results published for some organic PCMs [18, 19, 21, 40] with tenths of percent of material with high thermal conductivity. But this is because the MNH itself has higher

thermal conductivity compared to organic PCMs tested and the addition of carbon is low. Thanks to small addition of carbon, the value of ΔH is maintained.

4. Conclusions

The carbon nanomaterial was added into magnesium chloride hexahydrate or magnesium nitrate hexahydrate to achieve the suppression of supercooling and improving of the thermal conductivity. However, the mixtures based on magnesium chloride hexahydrate demonstrate no positive effect on supercooling or even its deterioration. On contrary, the mixtures based on magnesium nitrate hexahydrate in all cases show significant decrease of supercooling. The best results were obtained for mixture with graphite or graphene. During the fifty cycles of charging/discharging an average value of enthalpy of phase transition similar to pure MNH was observed and the supercooling was only 2.2 and 2.6 °C for mixtures of MNH with 2 mass% of graphite and 3 mass% of graphene, respectively. The thermal conductivity measurement shows that the application of pressure during the preparation of the sample leads to significant increase of thermal conductivity of about 60 % comparing sample prepared without any pressure and 5 MPa. The addition of 3 mass% of graphene into MNH increased the thermal conductivity of about 9 % and even higher increase of 15 % was observed for mixture with 3 mass% of graphite. From a heat transfer point of view, the PCMs can improved their thermal conductivity either by application of higher pressure or addition of substance with better thermal conductivity as graphite.

References

[1] S.A. Mohamed, F.A. Al-Sulaiman, N.I. Ibrahim, M.H. Zahir, A. Al-Ahmed, R. Saidur, B.S. Yilbas, A.Z. Sahin, A review on current status and challenges of inorganic phase change materials for thermal energy storage systems, Renew Sust Energ Rev 70 (2017) 1072-1089. https://doi.org/10.1016/j.rser.2016.12.012.

[2] G. Alva, L.K. Liu, X. Huang, G.Y. Fang, Thermal energy storage materials and systems for solar energy applications, Renew Sust Energ Rev 68 (2017) 693-706. https://doi.org/10.1016/j.rser.2016.10.021.

[3] B. Zalba, J.M. Marin, L.F. Cabeza, H. Mehling, Review on thermal energy storage with phase change: materials, heat transfer analysis and applications, Appl Therm Eng 23(3) (2003) 251-283. https://doi.org/10.1016/S1359-4311(02)00192-8.

[4] S.L. Liu, Y.C. Li, Y.Q. Zhang, Review on Heat Transfer Mechanisms and Characteristics in Encapsulated PCMs, Heat Transfer Eng 36(10) (2015) 880-901. https://doi.org/10.1080/01457632.2015.965093.

[5] S. Jegadheeswaran, S.D. Pohekar, Performance enhancement in latent heat thermal storage system: A review, Renew Sust Energ Rev 13(9) (2009) 2225-2244. https://doi.org/10.1016/j.rser.2009.06.024.

[6] H. Nikpourian, A.R. Bahramian, M. Abdollahi, On the thermal performance of a novel PCM nanocapsule: The effect of core/shell, Renew Energ 151 (2020) 322-331. https://doi.org/10.1016/j.renene.2019.11.027.

[7] H.W. Ryu, S.W. Woo, B.C. Shin, S.D. Kim, Prevention of Supercooling and Stabilization of Inorganic Salt Hydrates as Latent-Heat Storage Materials, Sol Energ Mat Sol C 27(2) (1992) 161-172. https://doi.org/10.1016/0927-0248(92)90117-8.

[8] P. Honcova, R. Pilar, V. Danielik, P. Soska, G. Sadovska, D. Honc, Suppressing supercooling in magnesium nitrate hexahydrate and evaluating corrosion of aluminium alloy container for latent heat storage application, J Therm Anal Calorim 129(3) (2017) 1573-1581. https://doi.org/10.1007/s10973-017-6334-0.

[9] G. Li, B.B. Zhang, X. Li, Y. Zhou, Q.G. Sun, Q. Yun, The preparation, characterization and modification of a new phase change material: CaCl2 center dot 6H(2)O-MgCl2 center dot 6H(2)O eutectic hydrate salt, Sol Energ Mat Sol C 126 (2014) 51-55. https://doi.org/10.1016/j.solmat.2014.03.031.

[10] L.P. Guo, X.P. Yu, D.L. Gao, Y.F. Guo, C. Ma, T.L. Deng, Synthesis and thermal energy storage properties of a calcium-based room temperature phase change material for energy storage, J Therm Anal Calorim 135(6) (2019) 3215-3221. https://doi.org/10.1007/s10973-018-7610-3.

[11] N. Beaupere, U. Soupremanien, L. Zalewski, Nucleation triggering methods in supercooled phase change materials (PCM), a review, Thermochim Acta 670 (2018) 184-201. https://doi.org/10.1016/j.tca.2018.10.009.

[12] M.Q. Li, Z.Q. Lin, Y.J. Sun, F.P. Wu, T. Xu, H.J. Wu, X.Q. Zhou, D.J. Wang, Y.F. Liu, Preparation and characterizations of a novel temperature-tuned phase change material based on sodium acetate trihydrate for improved performance of heat pump systems, Renew Energ 157 (2020) 670-677. https://doi.org/10.1016/j.renene.2020.05.061.

[13] R. Raud, R. Jacob, F. Bruno, G. Will, T.A. Steinberg, A critical review of eutectic salt property prediction for latent heat energy storage systems, Renew Sust Energ Rev 70 (2017) 936-944. https://doi.org/10.1016/j.rser.2016.11.274.

[14] N.I. Ibrahim, F.A. Al-Sulaiman, S. Rahman, B.S. Yilbas, A.Z. Sahin, Heat transfer enhancement of phase change materials for thermal energy storage applications: A critical review, Renew Sust Energ Rev 74 (2017) 26-50. https://doi.org/10.1016/j.rser.2017.01.169.

[15] K. Cornwell, Thermal Conductivity of Molten Salts, J Phys D Appl Phys 4(3) (1971) 441-&. https://iopscience.iop.org/article/10.1088/0022-3727/4/3/313/pdf.

[16] R. Nikolic, K. Kelic, O. Neskovic, The Thermal-Conductivities of Some Low Melting Materials Relevant to Energy-Storage, Appl Phys a-Mater 34(3) (1984) 199-203. https://doi.org/10.1007/BF00616920.

[17] K. Nithyanandam, R. Pitchumani, A. Mathur, Analysis of a latent thermocline storage system with encapsulated phase change materials for concentrating solar power, Appl Energ 113 (2014) 1446-1460. https://doi.org/10.1016/j.apenergy.2013.08.053.

[18] M. Dannemand, J.B. Johansen, S. Furbo, Solidification behavior and thermal conductivity of bulk sodium acetate trihydrate composites with thickening agents and graphite, Sol Energ Mat Sol C 145 (2016) 287-295. https://doi.org/10.1016/j.solmat.2015.10.038.

[19] D. Haillot, S. Pincemin, V. Goetz, D.R. Rousse, X. Py, Synthesis and characterization of multifunctional energy composite: Solar absorber and latent heat storage material of high thermal conductivity, Sol Energ Mat Sol C 161 (2017) 270-277. https://doi.org/10.1016/j.solmat.2016.12.010.

[20] W. Li, J.J. Klemes, Q.W. Wang, M. Zeng, Development and characteristics analysis of salt-hydrate based composite sorbent for low-grade thermochemical energy storage, Renew Energ 157 (2020) 920-940. https://doi.org/10.1016/j.renene.2020.05.062.

[21] Y.B. Cui, C.H. Liu, S. Hu, X. Yu, The experimental exploration of carbon nanofiber and carbon nanotube additives on thermal behavior of phase change materials, Sol Energ Mat Sol C 95(4) (2011) 1208-1212. https://doi.org/10.1016/j.solmat.2011.01.021.

[22] H.Z. Ke, Z.Y. Pang, Y.F. Xu, X.D. Chen, J.P. Fu, Y.B. Cai, F.L. Huang, Q.F. Wei, Graphene oxide improved thermal and mechanical properties of electrospun methyl stearate/polyacrylonitrile form-stable phase change composite nanofibers, J Therm Anal Calorim 117(1) (2014) 109-122. https://doi.org/10.1007/s10973-014-3669-7.

[23] J.L. Zeng, Z. Cao, D.W. Yang, L.X. Sun, L. Zhang, Thermal conductivity enhancement of Ag nanowires on an organic phase change material, J Therm Anal Calorim 101(1) (2010) 385-389. https://doi.org/10.1007/s10973-009-0472-y.

[24] W.L. Cui, Y.P. Yuan, L.L. Sun, X.L. Cao, X.J. Yang, Experimental studies on the supercooling and melting/freezing characteristics of nano-copper/sodium acetate trihydrate composite phase change materials, Renew Energ 99 (2016) 1029-1037. https://doi.org/10.1016/j.renene.2016.08.001.

[25] L.W. Fan, J.M. Khodadadi, Thermal conductivity enhancement of phase change materials for thermal energy storage: A review, Renew Sust Energ Rev 15(1) (2011) 24-46. https://doi.org/10.1016/j.rser.2010.08.007.

[26] L.F. Cabeza, H. Mehling, S. Hiebler, F. Ziegler, Heat transfer enhancement in water when used as PCM in thermal energy storage, Appl Therm Eng 22(10) (2002) 1141-1151. https://doi.org/10.1016/S1359-4311(02)00035-2.

[27] G.S. Wei, G. Wang, C. Xu, X. Ju, L.J. Xing, X.Z. Du, Y.P. Yang, Selection principles and thermophysical properties of high temperature phase change materials for thermal energy storage: A review, Renew Sust Energ Rev 81 (2018) 1771-1786. https://doi.org/10.1016/j.rser.2017.05.271.

[28] C. Veerakumar, A. Sreekumar, Phase change material based cold thermal energy storage: Materials, techniques and applications - A review, Int J Refrig 67 (2016) 271-289. https://doi.org/10.1016/j.ijrefrig.2015.12.005.

[29] L. Qiu, Y.X. Ouyang, Y.H. Feng, X.X. Zhang, Review on micro/nano phase change materials for solar thermal applications, Renew Energ 140 (2019) 513-538. https://doi.org/10.1016/j.renene.2019.03.088.

[30] C. Li, Q. Li, Y.L. Ding, Carbonate salt based composite phase change materials for medium and high temperature thermal energy storage: From component to device level performance through modelling, Renew Energ 140 (2019) 140-151. https://doi.org/10.1016/j.renene.2019.03.005.

[31] M.K. Saranprabhu, K.S. Rajan, Magnesium oxide nanoparticles dispersed solar salt with improved solid phase thermal conductivity and specific heat for latent heat thermal energy storage, Renew Energ 141 (2019) 451-459. https://doi.org/10.1016/j.renene.2019.04.027.

[32] A. Vasu, F.Y. Hagos, M.M. Noor, R. Mamat, W.H. Azmi, A.A. Abdullah, T.K. Ibrahim, Corrosion effect of phase change materials in solar thermal energy storage

application, Renew Sust Energ Rev 76 (2017) 19-33. https://doi.org/10.1016/j.rser.2017.03.018.

[33] L. Calabrese, V. Brancato, V. Paolomba, E. Proverbio, An experimental study on the corrosion sensitivity of metal alloys for usage in PCM thermal energy storages, Renew Energ 138 (2019) 1018-1027. https://doi.org/10.1016/j.renene.2019.02.013.

[34] E. Oro, L. Miro, C. Barreneche, I. Martorell, M.M. Farid, L.F. Cabeza, Corrosion of metal and polymer containers for use in PCM cold storage, Appl Energ 109 (2013) 449-453. https://doi.org/10.1016/j.apenergy.2012.10.049.

[35] T. Nomura, K. Tabuchi, C.Y. Zhu, N. Sheng, S.F. Wang, T. Akiyama, High thermal conductivity phase change composite with percolating carbon fiber network, Appl Energ 154 (2015) 678-685. https://doi.org/10.1016/j.apenergy.2015.05.042.

[36] X.B. Gu, P. Liu, L. Bian, H.C. He, Enhanced thermal conductivity of palmitic acid/mullite phase change composite with graphite powder for thermal energy storage, Renew Energ 138 (2019) 833-841. https://doi.org/10.1016/j.renene.2019.02.031.

[37] M.D. Yuan, Y.X. Ren, C. Xu, F. Ye, X.Z. Du, Characterization and stability study of a form-stable erythritol/expanded graphite composite phase change material for thermal energy storage, Renew Energ 136 (2019) 211-222. https://doi.org/10.1016/j.renene.2018.12.107.

[38] Q.Q. Wang, D. Zhou, Y.M. Chen, P. Eames, Z.G. Wu, Characterization and effects of thermal cycling on the properties of paraffin/expanded graphite composites, Renew Energ 147 (2020) 1131-1138. https://doi.org/10.1016/j.renene.2019.09.091.

[39] C.C. Li, B.S. Xie, Z.X. He, J. Chen, Y. Long, 3D structure fungi-derived carbon stabilized stearic acid as a composite phase change material for thermal energy storage, Renew Energ 140 (2019) 862-873. https://doi.org/10.1016/j.renene.2019.03.121.

[40] U.N. Temel, S. Kurtulus, M. Parlak, K. Yapici, Size-dependent thermal properties of multi-walled carbon nanotubes embedded in phase change materials, J Therm Anal Calorim 132(1) (2018) 631-641. https://doi.org/10.1007/s10973-018-6966-8.

[41] S. Mesgari, R.A. Taylor, N.E. Hjerrild, F. Crisostomo, Q.Y. Li, J. Scott, An investigation of thermal stability of carbon nanofluids for solar thermal applications, Sol Energ Mat Sol C 157 (2016) 652-659. https://doi.org/10.1016/j.solmat.2016.07.032.

[42] A. Sari, A. Al-Ahmed, A. Bicer, F.A. Al-Sulaiman, G. Hekimoglu, Investigation of thermal properties and enhanced energy storage/release performance of silica fume/myristic acid composite doped with carbon nanotubes, Renew Energ 140 (2019) 779-788. https://doi.org/10.1016/j.renene.2019.03.102.

[43] Z. Jiang, T. Ouyang, Y. Yang, L. Chen, X.H. Fan, Y.B. Chen, W.W. Li, Y.Q. Fei, Thermal conductivity enhancement of phase change materials with form-stable carbon bonded carbon fiber network, Mater Design 143 (2018) 177-184. https://doi.org/10.1016/j.matdes.2018.01.052.

[44] S.Y. Zhou, Y. Zhou, Z.Y. Ling, Z.G. Zhang, X.M. Fang, Modification of expanded graphite and its adsorption for hydrated salt to prepare composite PCMs, Appl Therm Eng 133 (2018) 446-451. https://doi.org/10.1016/j.applthermaleng.2018.01.067.

[45] Z.J. Duan, H.Z. Zhang, L.X. Sun, Z. Cao, F. Xu, Y.J. Zou, H.L. Chu, S.J. Qiu, C.L. Xiang, H.Y. Zhou, CaCl2 center dot 6H(2)O/Expanded graphite composite as form-stable phase change materials for thermal energy storage, J Therm Anal Calorim 115(1) (2014) 111-117. https://doi.org/10.1007/s10973-013-3311-0.

[46] R.D. Ye, W.Z. Lin, K.J. Yuan, X.M. Fang, Z.G. Zhang, Experimental and numerical investigations on the thermal performance of building plane containing CaCl2 center dot 6H(2)O/expanded graphite composite phase change material, Appl Energ 193 (2017) 325-335. https://doi.org/10.1016/j.apenergy.2017.02.049.

[47] X. Li, Y. Zhou, H.E. Nian, X.F. Ren, O.Y. Dong, C.X. Hai, Y. Shen, J.B. Zeng, Phase change behavior of latent heat storage media based on calcium chloride hexahydrate composites containing strontium chloride hexahydrate and oxidation expandable graphite, Appl Therm Eng 102 (2016) 38-44. https://doi.org/10.1016/j.applthermaleng.2016.03.098.

[48] Y.S. Liu, Y.Z. Yang, Form-stable phase change material based on Na2CO3 center dot 10H(2)O-Na2HPO4 center dot 12H(2)O eutectic hydrated salt/expanded graphite oxide composite: The influence of chemical structures of expanded graphite oxide, Renew Energ 115 (2018) 734-740. ttps://doi.org/10.1016/j.renene.2017.08.097.

[49] J. Fukai, M. Kanou, Y. Kodama, O. Miyatake, Thermal conductivity enhancement of energy storage media using carbon fibers, Energ Convers Manage 41(14) (2000) 1543-1556. https://doi.org/10.1016/S0196-8904(99)00166-1.

[50] F. Frusteri, V. Leonardi, S. Vasta, G. Restuccia, Thermal conductivity measurement of a PCM based storage system containing carbon fibers, Appl Therm Eng 25(11-12) (2005) 1623-1633. https://doi.org/10.1016/j.applthermaleng.2004.10.007.

[51] S.F. Wu, T. Yan, Z.H. Kuai, W.G. Pan, Preparation and thermal property analysis of a novel phase change heat storage material, Renew Energ 150 (2020) 1057-1065. https://doi.org/10.1016/j.renene.2019.11.002.

[52] R. Pilar, L. Svoboda, P. Honcova, L. Oravova, Study of magnesium chloride hexahydrate as heat storage material, Thermochim Acta 546 (2012) 81-86. https://doi.org/10.1016/j.tca.2012.07.021.

[53] G. Sadovska, P. Honcova, R. Pilar, L. Oravova, D. Honc, Calorimetric study of calcium nitrate tetrahydrate and magnesium nitrate hexahydrate, J Therm Anal Calorim 124(1) (2016) 539-546. https://doi.org/10.1007/s10973-015-5159-y.

[54] H. Schmit, C. Rathgeber, P. Hoock, S. Hiebler, Critical review on measured phase transition enthalpies of salt hydrates in the context of solid-liquid phase change materials, Thermochim Acta 683 (2020). https://doi.org/10.1016/j.tca.2019.178477.

[55] P. Sazama, J. Pastvova, C. Rizescu, A. Tirsoaga, V.I. Parvulescu, H. Garcia, L. Kobera, J. Seidel, J. Rathousky, P. Klein, I. Jirka, J. Moravkova, V. Blechta, Catalytic Properties of 3D Graphene-Like Microporous Carbons Synthesized in a Zeolite Template, Acs Catal 8(3) (2018) 1779-1789. https://doi.org/10.1021/acscatal.7b04086. https://doi.org/10.1021/acscatal.7b04086.

[56] Application note TN149 - Heat Capacity determination, Setaram. https://www.setaram.com/application-notes/tn149-heat-capacity-determination/.

[57] S.C. Mraw, D.F. Naas, Measurement of Accurate Heat-Capacities by Differential Scanning Calorimetry Comparison of Dsc Results on Pyrite (100-K to 800-K) with Literature Values from Precision Adiabatic Calorimetry, J Chem Thermodyn 11(6) (1979) 567-584. https://doi.org/10.1016/0021-9614(79)90097-1.

[58] Manufacturer information available at: https://ctherm.com/products/tci_thermal_conductivity/how_the_tci_works/mtps/.

[59] M. Kenisarin, K. Mahkamov, Salt hydrates as latent heat storage materials:Thermophysical properties and costs, Sol Energ Mat Sol C 145 (2016) 255-286. https://doi.org/10.1016/j.solmat.2015.10.029.

[60] International Zeolite Association - Database of Zeolite Structures available at http://www.iza-structure.org/databases/.
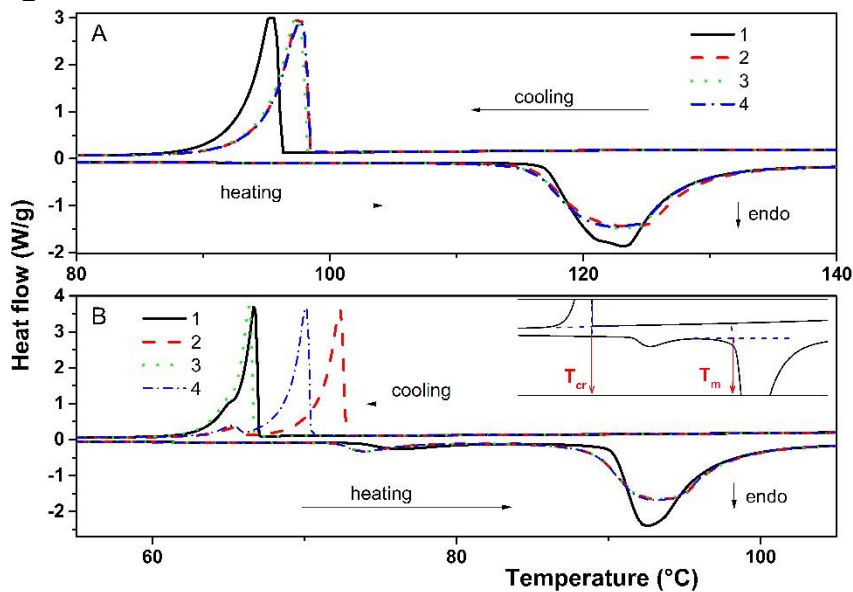
Figures

Fig. 1 Slow four DSC scans (heating 4 K/min, cooling 2K/min) obtained for A) MCH and B) MNH. The inserted figure in B depicts the evaluation of onset temperatures (temperature of melting T_m, temperature of crystallization T_{cr}).
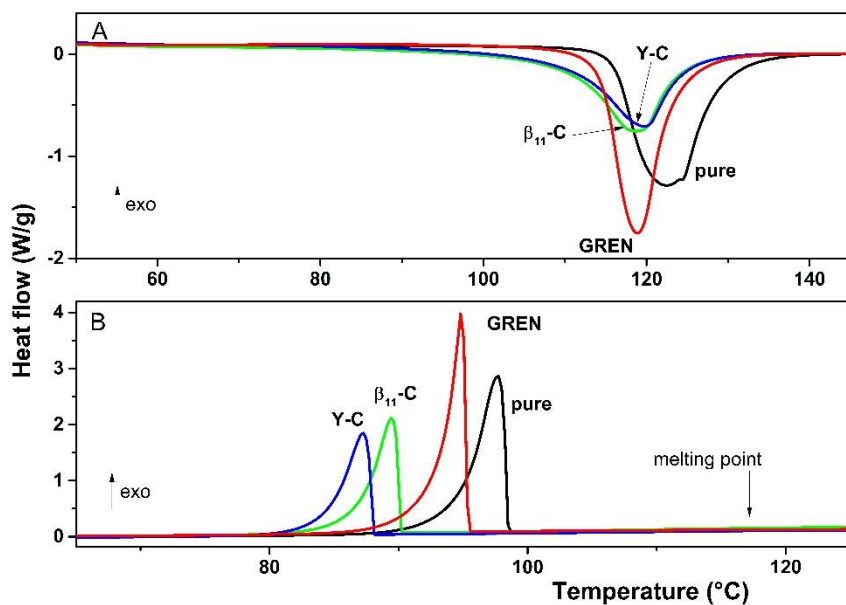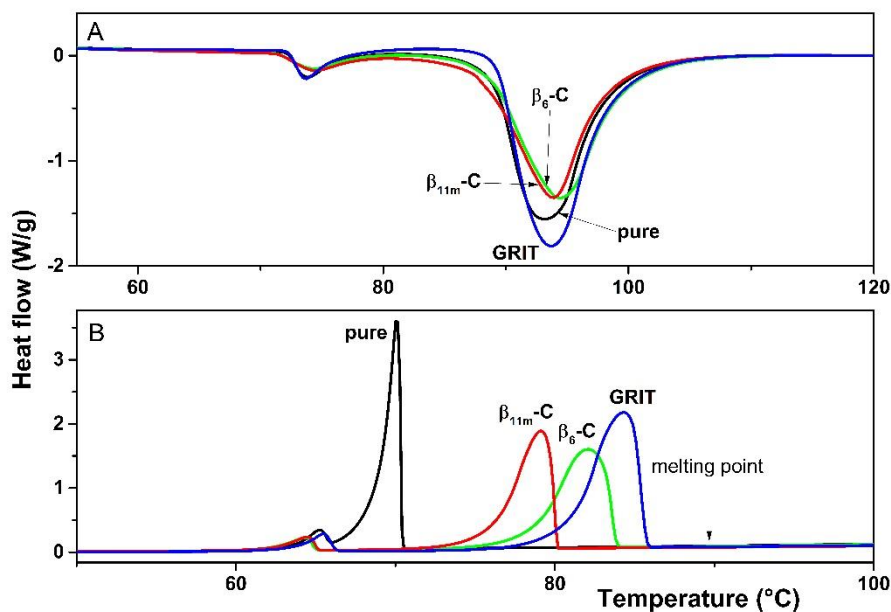

Fig. 2 The DSC peaks of the 4th heating (A) and cooling (B) scan from the slow four cycles (heating 4 K/min, cooling 2K/min) of pure MCH and its mixtures with 3 mass% of given carbon material.
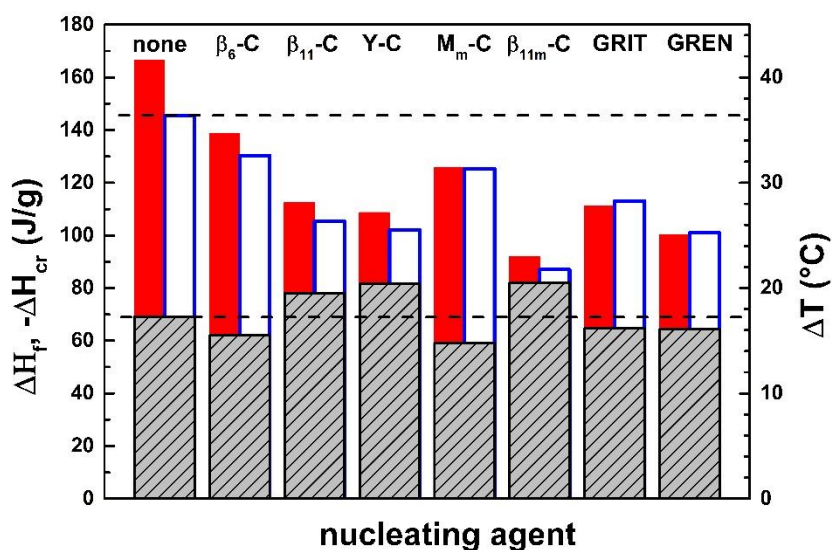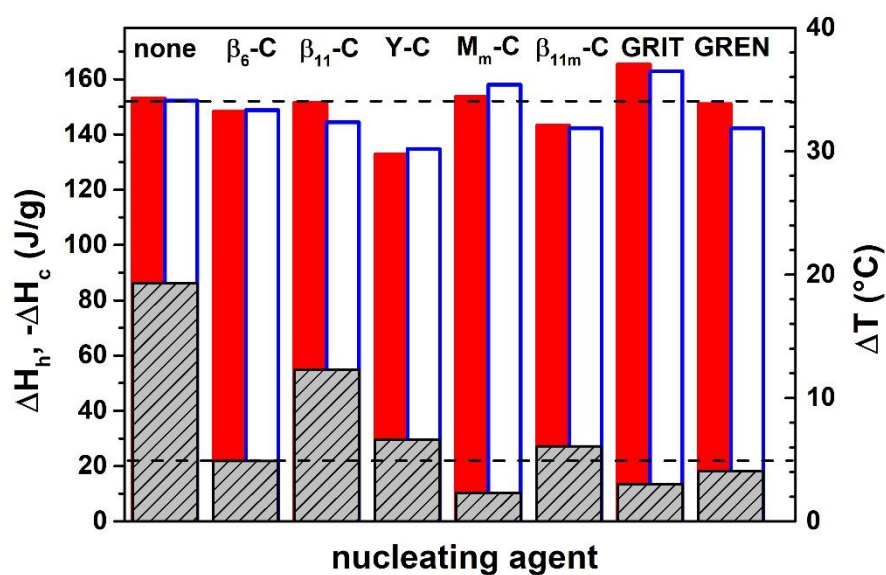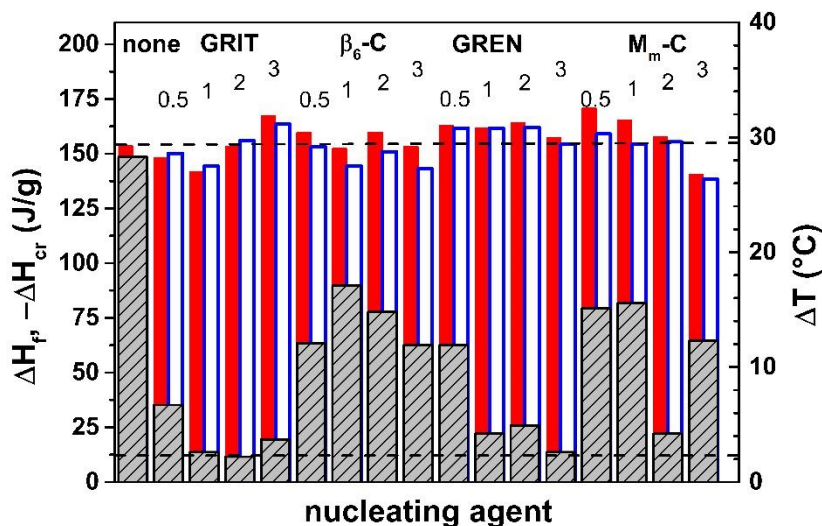
1
2   **Fig. 3**   The average value of heat of fusion (full red column) and crystallization (empty blue
3   column) and the supercooling (striped grey column) for pure MCH and its mixture with 3
4   mass% of each carbon nanomaterial.
5
6

7
8   **Fig. 4**   The illustration of DSC peaks of the 4th heating (A) and cooling (B) scan from the slow
9   four cycles (heating 4 K/min, cooling 2K/min) of pure MNH and its mixtures with 3 mass% of
10 given carbon material.
11
12

Fig. 5 The average values of heat effects observed during the heating (ΔH_h, full red column), the cooling (ΔH_c, empty blue column) and the supercooling (strips grey column) for pure MNH and its mixtures with 3 mass% of each carbon material calculated from 2nd, 3rd and 4th cycle of the slow DSC scans.


Fig. 6 The average value (from 2nd to 50th cycle) of heat of fusion (full red column), crystallization (empty blue column) and the supercooling (strips grey column) for pure MNH (data from Ref. [8] also for 49 evaluated cycles) and its mixtures with selected carbons (content from 0.5 to 3 mass%) from fast DSC measurements (heating rate of 10 K/min).
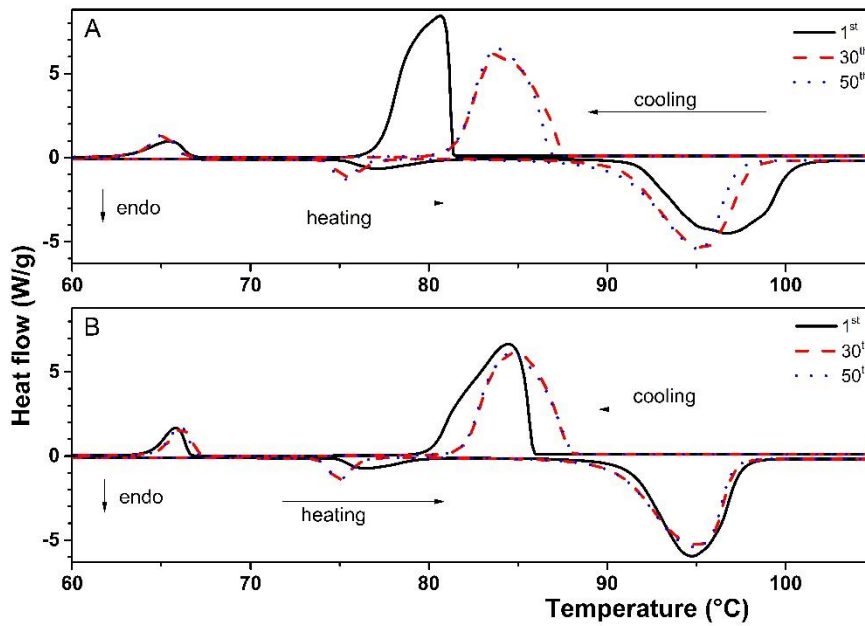
Fig. 7 DSC scans for the 1st, 30th and 50th cycle of MNH mixture with 2 mass% of A) M_m-C and B) GRIT.
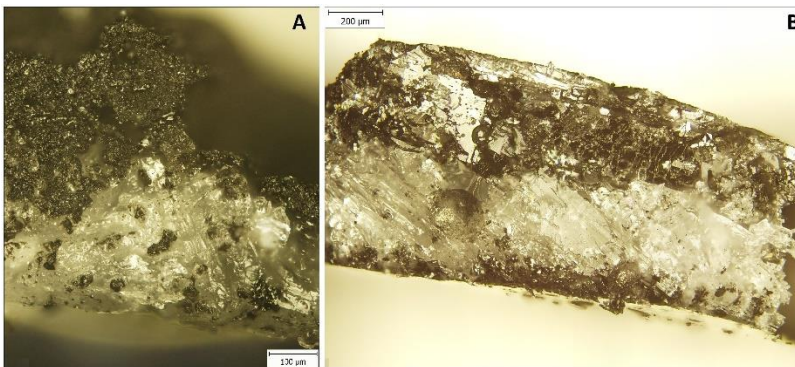
Fig. 8 Optical micrographs of sample after DSC measurement for MNH with A) 3 mass% of β_{11}-C after 4 slow cycles and B) 3 mass% of M_m-C after 50 cycles. MNH is white and the dark parts are carbon.

18
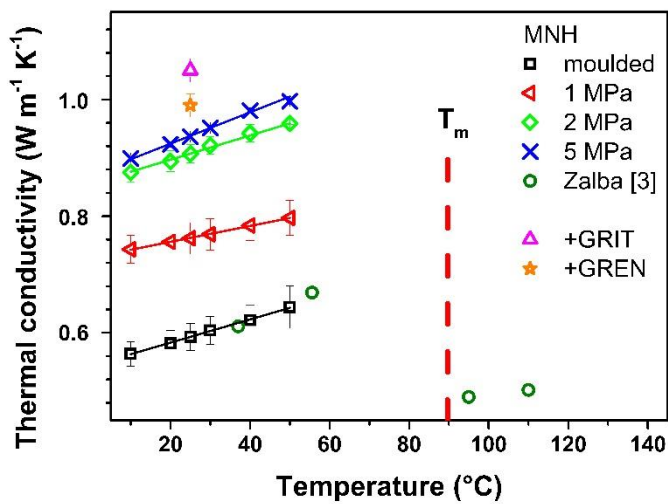
1 **Fig. 9** Temperature dependence of thermal conductivity of MNH in the compact form –
2 moulded sample and pellets prepared under the pressure of 1, 2 and 5 MPa (experimental
3 points and linear fit) with the 3 mass% GRIT and 3 mass% GREN tablets.
4
5

Tables

Table 1 Synthesized carbon samples and their characteristics: used zeolite template, carbon precursor, crystal size, surface area and flash point.

Sample	Acronym	Template/ (Si/Al)	Carbon precursor	Crystal size [nm]	Surface area [m²/g]	Flash-point onset/T_{max} [°C]
β_6 – carbon	β_6-C	synthesized Al-rich *BEA/5.6	furfuryl alcohol	200-300	494	468/585
β_{11} – carbon *	β_{11}-C	commercial *BEA/11.3	propylene	300-500	2454	433/517
Y-carbon *	Y-C	Commercial FAU/6	propylene	300-1000	2443	473/543
M_m-carbon	M_m-C	commercial MOR/12 treated to be mesoporous	propylene	150-300	421	495/637
β_{11m} – carbon	β_{11m}-C	commercial *BEA/11.3 treated to be mesoporous	propylene	300-500	1473	450/593
graphite	GRIT	-	-	$3 \cdot 10^4 - 10^5$	8	547/805
graphene	GREN	-	-	$3 \cdot 10^3 - 6 \cdot 10^3$	2630	350/407

*Detail description of synthesis and characterization is published in [49], where β_{11}-C is referred as β-carbon and Y-C as Y-carbon.

Table 2 Effusivity, *e,* and thermal conductivity, *k,* of samples in the form of powder, the value of density (bulk density ρ_b and tapped density ρ_t) and heat capacity at 25 °C used for recalculation of *e* into *k*.

sample	*e* [W s$^{1/2}$/m² K]	ρ_b [kg/m³]	ρ_t [kg/m³]	C_p [J/kg K]	*k* [W/m K]
MNH	165 ± 6* 241 ± 15**	1653 ± 8	807 ± 11* 974 ± 16**	1733 [48]	0.07 ± 0.01* 0.09 ± 0.01**
GRIT	201 ± 7	2524 ± 41	602 ± 12	742 ± 4	0.08 ± 0.01
GREN	264 ± 8	2267 ± 37	702 ± 11	711 ± 4	0.09 ± 0.01
MNH+3 mass% GRIT	318 ± 8	1674 ± 5	920 ± 19	1676 ± 8	0.11 ± 0.01
MNH+3 mass% GREN	333 ± 8	1670 ± 8	965 ± 18	1682 ± 8	0.11 ± 0.01

* original crystal size $2100 – 2500$ μm; ** reduced crystal size $150 – 600$ μm

Table 3 Effusivity, *e*, thermal conductivity *k* and density of samples in compact form (ρ_c) of pellets or moulded samples (pure MNH) determined at temperature of 25 °C.

sample	Pressure [MPa]	*e* [W s$^{1/2}$/m² K]	ρ_c [kg/m]	*k* [W/m K]

MNH	-	948 ± 23	1463 ± 31	0.59 ± 0.02
	1	1109 ± 25	1514 ± 14	0.76 ± 0.03
	2	1243 ± 14	1609 ± 5	0.91 ± 0.02
	5	1269 ± 5	1635 ± 5	0.94 ± 0.01
MNH + 3 mass% GRIT	2	1370 ± 10	1625 ± 5	1.05 ± 0.02
MNH + 3 mass% GREN	2	1311 ± 10	1628 ± 5	0.99 ± 0.02

Table 4 The parameters of linear dependence of k on temperature obtained by fitting data in Fig. 9 for MNH compact samples, the value of coefficient of determination (R^2) is given.

Pressure [MPa]	Slope [10^{-3} W/ m K^2]	Section [W/ m K]	R^2
-	1.99 ± 0.04	0.543 ± 0.001	0.998
1	1.36 ± 0.02	0.729 ± 0.001	0.999
2	2.07 ± 0.05	0.855 ± 0.003	0.997
5	2.69 ± 0.06	0.871 ± 0.002	0.997

Improvement of thermal energy accumulation by incorporation of carbon nanomaterial into magnesium chloride hexahydrate and magnesium nitrate hexahydrate
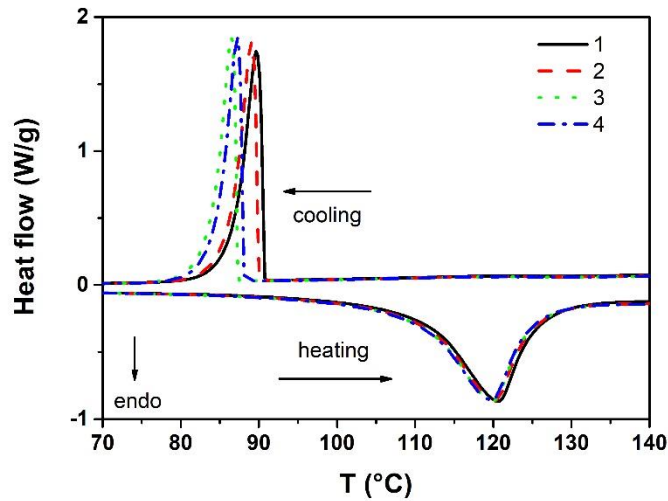

Fig. S1. DSC scans for the slow four cycles (heating 4 K/min, cooling 2 K/min) of MCH with addition of 3 mass% of Y-C.
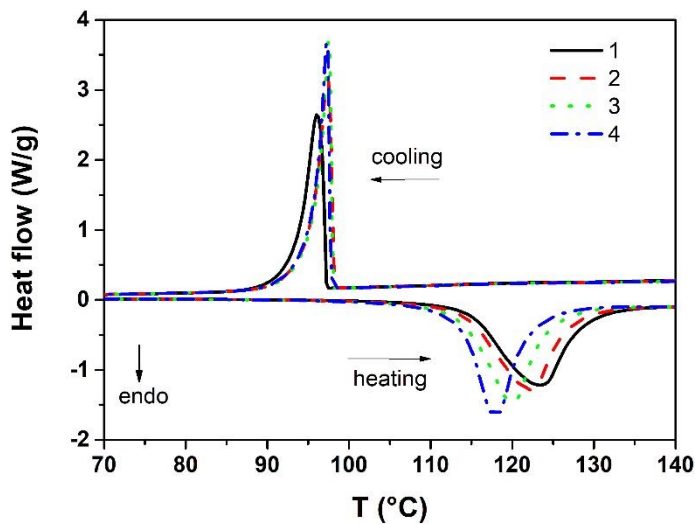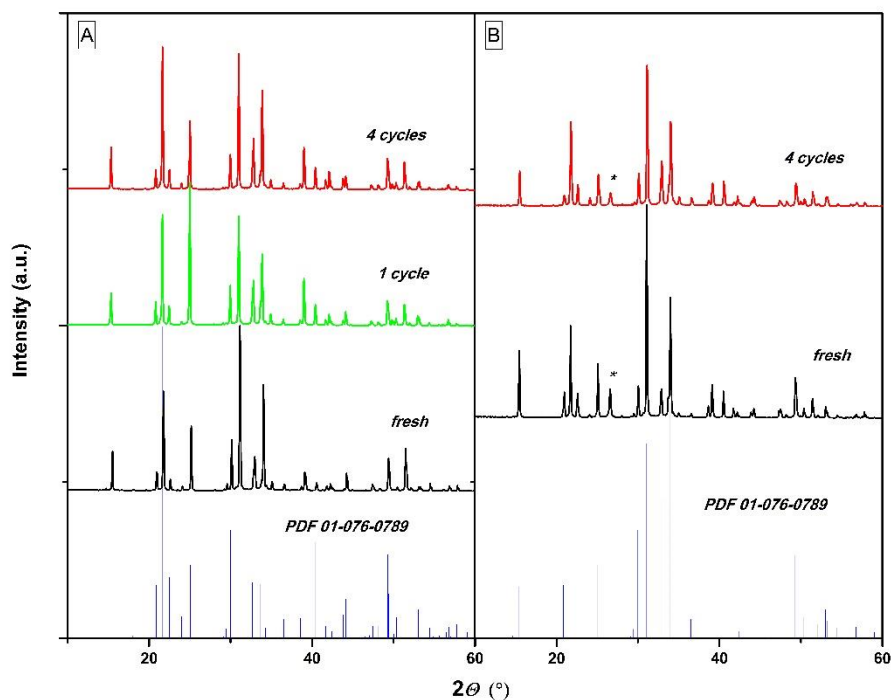

Fig. S2. DSC scans for the slow four cycles (heating 4 K/min, cooling 2 K/min) of MCH with addition of 3 mass% of β_6-C.

Fig. S3. The X-ray diffraction lines of A) MCH, B) MCH + 3 % GREN (the line signed "*" corresponds to the carbon strongest line).

Table S1. The 5 strongest X-ray diffraction lines for Mg-Cl salts.

Compound	2θ in degree $^{(intensity)}$				
	1	2	3	4	5
MCH	$21.7^{(999)}$	$33.9^{(752)}$	$31.0^{(622)}$	$32.8^{(446)}$	$30.0^{(346)}$
MCT	$29.4^{(999)}$	$41.1^{(777)}$	$32.3^{(770)}$	$33.6^{(641)}$	$40.9^{(598)}$
MCD	$32.0^{(999)}$	$15.9^{(602)}$	$20.7^{(503)}$	$32.4^{(474)}$	$37.4^{(377)}$
MC	$35.0^{(999)}$	$15.0^{(527)}$	$30.1^{(361)}$	$50.4^{(257)}$	$50.1^{(233)}$
MHC	$15.2^{(999)}$	$32.2^{(617)}$	$40.1^{(391)}$	$54.1^{(170)}$	$47.7^{(121)}$